1046 *Chem. Mater.* **2010,** *22,* 1046–1053
DOI:10.1021/cm902001c

CHEMISTRY OF MATERIALS
Article

High Figure of Merit in Nanostructured n-Type KPb_mSbTe_{m+2} Thermoelectric Materials[†]

Pierre F. P. Poudeu,[‡] Aurélie Guéguen,[‡] Chun-I Wu,[∥] Tim Hogan,[∥] and Mercouri G. Kanatzidis*[,‡,§]

[‡]*Department of Chemistry, Northwestern University, Evanston, Illinois 60208,* [§]*Materials Science Division, Argonne National Laboratory, Argonne, Illinois 60439, and* [∥]*Department of Electrical and Computer Engineering, Michigan State University, East Lansing, Michigan 48824*

Received July 5, 2009. Revised Manuscript Received August 19, 2009

We demonstrate that the KPb_mSbTe_{2+m} system (PLAT-*m* for tellurium, antimony, lead potassium, $m = 19-21$) of materials exhibits high thermoelectric performance. Samples with compositions $K_{1-x}Pb_{m+\delta}Sb_{1+\gamma}Te_{m+2}$ were prepared using several combinations of x, δ, γ and m and their thermoelectric properties were investigated in the temperature range of 300 − 800 K. All $K_{1-x}Pb_{m+\delta}Sb_{1+\gamma}Te_{m+2}$ samples exhibited n-type conduction over the measured temperature range. Their lattice thermal conductivities were found to be significantly reduced when compared to PbTe and even $AgPb_mSbTe_{m+2}$. For example, for $K_{0.95}Pb_{20}Sb_{1.2}Te_{22}$ a lattice thermal conductivity as low as 0.4 W/(m·K) was estimated at 650 K (based on a Lorenz number of 1.25×10^{-8} W·Ω/K^2). High resolution transmission electron microscopy on several samples revealed a widely dispersed nanoscale particle with varying size and shape endotaxially embedded inside a PbTe-rich matrix which is believed to be responsible for the reduced lattice thermal conductivity of $K_{1-x}Pb_{m+\delta}Sb_{1+\gamma}Te_{m+2}$ materials. Because of their small size, the nanoinclusions are coherent with the matrix and therefore do not markedly degrade the electrical conductivity of the materials. As a result, very high figures of merit are achieved at high temperature for several compositions. For $K_{0.95}Pb_{20}Sb_{1.2}Te_{22}$, a maximum figure of merit ZT ∼ 1.6 was obtained around 750 K. This value is similar to that of n-type LAST-18 and is two times larger than that of the-state-of-the-art n-type PbTe.

Introduction

Designing new thermoelectric materials with high figure of merit[1] continues to be the target of fundamental research. Bulk materials featuring nanometer scale inclusions represent emerging alternatives to the layer-by-layer top-down methods for high performance thermoelectrics. It has been demonstrated that the presence of nanometer length scale inclusions in bulk materials can significantly reduce the lattice component of the thermal conductivity.[2−7] Thermal conductivity reductions have been predicted in nanostructures even for periodicities of tens to hundreds of nanometers.[8] Significant thermal conductivity reduction can occur regardless of the orientation of the nanostructures relative to the measurement direction. Thus, randomly oriented structures with nanometer to submicrometer sizes embedded inside bulk thermoelectric materials can be anticipated to result in enhancements of the figure of merit (ZT) through severe suppression of the lattice thermal conductivity. The nanocomponents can play an important role in scattering mid-to-long wavelength phonons at high temperature, thus reducing the lattice thermal conductivity. Critical in this research are the judicious choice of the nanocomponents (which can be an element or a compound) and most importantly the synthetic approach used to uniformly insert nanosized inclusions inside the bulk matrix. There are considerable efforts under way to develop synthesis routes to nanostructured bulk thermoelectric materials.[3,4,9−15] For example, nanostructured PbTe bulk thermoelectric materials could be

[†] Accepted as part of the 2010 "Materials Chemistry of Energy Conversion Special Issue".

*Corresponding author. Tel: +1-847-467-1541. Fax: +1-847-491-5937. E-mail: m-kanatzidis@northwestern.edu.

(1) The performance of thermoelectric materials is defined by its figure of merit $ZT = (\sigma S^2)T/\kappa$, where S is the Seebeck coefficient, σ is the electrical conductivity, κ is the total thermal conductivity, and T is the absolute temperature. The numerator is called the power factor. The thermal conductivity κ is expressed as a sum of the phonon κ_{ph} and electronic contribution κ_{el}.

(2) Kim, W.; Zide, J.; Gossard, A.; Klenov, D.; Stemmer, S.; Shakouri, A.; Majumdar, A. *Phys. Rev. Lett.* **2006**, *96*, 045901.
(3) Poudeu, P. F. P.; DAngelo, J.; Kong, H.; Downey, A. D.; Short, J. L.; Pcionek, R.; Hogan, T. P.; Uher, C.; Kanatzidis, M. G. *J. Am. Chem. Soc.* **2006**, *126*, 14347–14355.
(4) Hsu, K. F.; Loo, S.; Guo, F.; Chen, W.; Dyck, J. S.; Uher, C.; Hogan, T.; Polychroniadis, E. K.; Kanatzidis, M. G. *Science* **2004**, *303*, 818–821.
(5) Quarez, E.; Hsu, K. F.; Pcionek, R.; Frangis, N.; Polychroniadis, E. K.; Kanatzidis, M. G. *J. Am. Chem. Soc.* **2005**, *127*, 9177–9190.
(6) Nolas, G. S.; Poon, J.; Kanatzidis, M. *MRS Bull.* **2006**, *31*, 199–205.
(7) Sootsman, J. R.; Pcionek, R. J.; Kong, H.; Uher, C.; Kanatzidis, M. G. *Chem. Mater.* **2006**, *18*, 4993–4995.
(8) Chen, G. *J. Heat Trans.* (*Transactions of the ASME*) **1997**, *119*, 220–229.
(9) Koh, Y. K.; Vineis, C. J.; Calawa, S. D.; Walsh, M. P.; Cahill, D. G. *Appl. Phys. Lett.* **2009**, *94*, 153101.
(10) Minnich, A. J.; Dresselhaus, M. S.; Ren, Z. F.; Chen, G. *Energy Environ. Sci.* **2009**, *2*, 466–479.

 Published on Web 09/15/2009

achieved through matrix encapsulation,[7,16] spinodal decomposition,[13,17,18] and nucleation and growth.[3,12,14] Several of these materials, for example, LAST-*m* ($AgPb_mSbTe_{m+2}$),[4,5,19−21] LASTT-*m* ($Ag(Pb_{1-y}Sn_y)_mSbTe_{m+2}$),[12] and SALT ($Na_{1-x}Pb_mSb_yTe_{m+2}$).[14,22] show enhancement of the thermoelectric figure of merit compared to pure PbTe and its nanostructure-free solid solutions.

Monovalent and alkali metal doped PbTe systems are very interesting for several reasons. Ab initio calculations within density functional theory (DFT) of PbTe with and without monovalent impurities (Na, K, Tl, Cu, and Ag) suggest an increase in the density of states (DOS) near the top of the valence band for Tl,[23] Cu, and Ag dopands while Na does not change the DOS within 0.5 eV of the band maxima.[24]

Our choice of Sb as one of the key elements was motivated by theoretical studies of the effect of Sb impurities on the electronic structure of PbTe. These suggested additional electronic states (resonance states) at the bottom of the conduction band and a possible enhancement of the thermopower for optimal Sb concentration.[25] Finally, we expected that the substitution of Ag in the LAST-*m* system (which makes covalent Ag−Te bonds in the structure) with K (which would make ionic K···Te bonds) would have a profound effect in the phase segregation processes in this PbTe matrix. For example, compositionally more abrupt interfaces between possible nanostructures and the matrix could form in the K based system. On the basis of the above arguments, alkali metal based materials could even lower lattice thermal conductivity when compared to the LAST-*m* materials. This hypothesis is already supported by the difference in the lattice thermal conductivity as well as the density of nanostructures observed on numerous transmission electron microscopy images of Ag-based materials $AgPb_mSbTe_{m+2}$,[4,5,20,21,26] $Ag(Pb_{1-y}Sn_y)_mSbTe_{m+2}$,[12] and Na-based materials $Na_{1-x}Pb_mSb_yTe_{m+2}$.[14,22]

In this paper, we present the thermoelectric properties of $K_{1-x}Pb_{m+\delta}Sb_{1+\gamma}Te_{m+2}$, the *hitherto* unexplored K-based analogues of the p-type $Na_{1-x}Pb_mSb_yTe_{m+2}$ materials. From the chemistry point of view, it is anticipated that the K-based materials will behave like the $Na_{1-x}Pb_mSb_yTe_{m+2}$ analogues given the similitude in the chemistry of K and Na compounds. However, the ab initio calculations results which revealed a very different behavior of the electronic structure of PbTe near the Fermi level when doped with Na or K strongly indicate the necessity of a full investigation of the thermoelectric properties of $K_{1-x}Pb_{m+\delta}Sb_{1+\gamma}Te_{m+2}$. We show that the K-based materials (PLAT-*m*: potassium−lead−antimony−tellurium) are unique. High-resolution transmission electron microscopy (HRTEM) images of selected samples showed that $K_{1-x}Pb_{m+\delta}Sb_{1+\gamma}Te_{m+2}$ materials are nanostructured similar to the p-type $Na_{1-x}Pb_mSb_yTe_{m+2}$ analogues.[14] These endotaxial[5] nanostructures result in a very low lattice thermal conductivity. All $K_{1-x}Pb_{m+\delta}Sb_{1+\gamma}Te_{m+2}$ samples show n-type semiconducting behavior as opposed to the p-type character of the $Na_{1-x}Pb_mSb_yTe_{m+2}$ analogues. Selected compositions exhibited remarkable improvement in the figure of merit as a result of the strong reduction of the lattice thermal conductivity. For example, a maximum $ZT \sim 1.6$ at 750 K was measured for n-type $K_{0.95}Pb_{20}Sb_{1.2}Te_{22}$.

Experimental section

Synthesis. Samples of $K_{1-x}Pb_{m+\delta}Sb_{1+\gamma}Te_{m+2}$ materials used for this investigation were prepared as polycrystalline ingots by combining elements in the desired stoichiometry. Approximately 20 g of the starting materials were used for the synthesis. Pb (99.99%), Te (99.999%), and Sb (99.999%) weighed under ambient atmosphere were loaded into carbon coated quartz tubes ($\varnothing_{OD}$ = 10 mm, length = 20 cm) and transferred into a nitrogen atmosphere glovebox where the desired amount of potassium was added. The tubes were flame-sealed under residual pressure of $\sim 10^{-4}$ Torr, placed into a tube furnace (mounted on a rocking table), and heated up to allow complete melting of all components at 1400 K. At the molten temperature, the furnace was allowed to rock backward and forward to facilitate complete mixing and homogeneity of the liquid phase. After two hours of rocking, the furnace was finally immobilized in a vertical position for the crystal growth. The furnace was slowly cooled from 1400 to 820 K in 84 h followed by a fast cool to room temperature.

The resulting ingots were sliced in disk-shape specimens with approximate thickness of 2.5 mm thick and diameter of 8 mm for thermal diffusivity measurements. Rectangular bars of specimens with approximate dimensions 2.5 mm × 2.5 mm × 7 mm for simultaneous measurement of the electrical conductivity and

(11) Poudel, B.; Hao, Q.; Ma, Y.; Lan, Y. C.; Minnich, A.; Yu, B.; Yan, X.; Wang, D. Z.; Muto, A.; Vashaee, D.; Chen, X. Y.; Liu, J. M.; Dresselhaus, M. S.; Chen, G.; Ren, Z. *Science* **2008**, *320*, 634–638.
(12) Androulakis, J.; Hsu, K. F.; Pcionek, R.; Kong, H.; Uher, C.; Dangelo, J. J.; Downey, A.; Hogan, T.; Kanatzidis, M. G. *Adv. Mater.* **2006**, *18*, 1170–+.
(13) Androulakis, J.; Lin, C. H.; Kong, H. J.; Uher, C.; Wu, C. I.; Hogan, T.; Cook, B. A.; Caillat, T.; Paraskevopoulos, K. M.; Kanatzidis, M. G. *J. Am. Chem. Soc.* **2007**, *129*, 9780–9788.
(14) Poudeu, P. F. P.; D'Angelo, J.; Downey, A. D.; Short, J. L.; Hogan, T. P.; Kanatzidis, M. G. *Angew. Chem., Int. Ed.* **2006**, *45*, 3835.
(15) Bux, S. K.; Blair, R. G.; Pawan, K.; Gogna, P. K.; Lee, H.; Chen, G.; Dresselhaus, M. S.; Kaner, R. B.; Fleurial, J. P. *Adv. Funct. Mater.* **2009**, *19*, 2445−2452.
(16) Heremans, J. P.; Thrush, C. M.; Morelli, D. T. *J. Appl. Phys.* **2005**, *98*.
(17) Salamancayoung, L.; Partin, D. L.; Heremans, J. *J. Appl. Phys.* **1988**, *63*, 1504–1508.
(18) Ikeda, T.; Ravi, V. A.; Collins, L. A.; Haile, S. M.; Snyder, G. J. *J. Electron. Mater.* **2007**, *36*, 716–720.
(19) Han, M. K.; Hoang, K.; Kong, H. J.; Pcionek, R.; Uher, C.; Paraskevopoulos, K. M.; Mahanti, S. D.; Kanatzidis, M. G. *Chem. Mater.* **2008**, *20*, 3512–3520.
(20) Zhou, M.; Li, J. F.; Kita, T. *J. Am. Chem. Soc.* **2008**, *130*, 4527–4532.
(21) Wang, H.; Li, J. F.; Nan, C. W.; Zhou, M.; Liu, W. S.; Zhang, B. P.; Kita, T. *Appl. Phys. Lett.* **2006**, 88.
(22) Gueguen, A.; Poudeu, P. F. P.; Li, C. P.; Moses, S.; Uher, C.; He, J. Q.; Dravid, V.; Paraskevopoulos, K. A.; Kanatzidis, M. G. *Chem. Mater.* **2009**, *21*, 1683–1694.
(23) Heremans, J. P.; Jovovic, V.; Toberer, E. S.; Saramat, A.; Kurosaki, K.; Charoenphakdee, A.; Yamanaka, S.; Snyder, G. J. *Science* **2008**, *321*, 554–557.
(24) Ahmad, S.; Mahanti, S. D.; Hoang, K.; Kanatzidis, M. G. *Phys. Rev. B* **2006**, *74*, 155205.
(25) Bilc, D.; Mahanti, S. D.; Hsu, K. F.; Quarez, Q.; Pcionek, R.; and Kanatzidis, M. G. *Phys. Rev. Lett.* **2004**, *93*(14), 146403/1–146403/4.
(26) Cook, B. A.; Kramer, M. J.; Harringa, J. L.; Han, M. K.; Chung, D. Y.; Kanatzidis, M. G. *Adv. Funct. Mater.* **2009**, *19*, 1254–1259.

thermopower were also cut from the ingot using a precision wire saw (South Bay Technology). The surfaces of the rectangular bars were mirror-like, polished with SiC sandpaper, washed with ethanol, and dried with acetone to remove any remaining particle from the surface before measurements.

X-ray Diffraction. Finely ground samples of $K_{1-x}Pb_{m+\delta}Sb_{1+\gamma}Te_{m+2}$ were examined by X-ray diffraction. Diffraction patterns were collected using a Cu Kα (λ = 1.54056 Å) radiation in reflection geometry on an Inel diffractometer equipped with a position sensitive detector and operating at 40 kV and 20 A.

Differential Thermal Analysis (DTA). The melting temperatures of $K_{1-x}Pb_{m+\delta}Sb_{1+\gamma}Te_{m+2}$ samples were determined by carrying out differential thermal analysis (DTA) measurements using a Shimadzu DTA-50 thermal analyzer. Approximately 30 mg of finely ground powder of the materials was sealed in a small quartz tube, and an equivalent amount of alumina (Al_2O_3) was sealed in an identical quartz tube to serve as a reference. The samples were heated to 1300 at 10 K/min, isothermed for 2 min, and then cooled to 400 K at a rate of 10 K/min. The temperature difference between the sample and the reference was monitored during two heating and cooling cycles. The endothermic peak temperatures are reported as the melting points.

Transmission Electron Microscopy. Several specimens from numerous samples of the $K_{1-x}Pb_{m+\delta}Sb_{1+\gamma}Te_{m+2}$ series were examined with transmission electron microscopy to assess their microstructure and to determine the size, shape, and distribution of the nanostructures inside the PbTe-rich matrix. Specimens used for the high resolution transmission electron microscopy (HRTEM) were prepared as described elsewhere.[14] HRTEM images were recorded at 200 kV using a JEOL JEM 2200FS (field emission TEM).

X-ray Fluorescence Analysis. The composition of the as-prepared ingots was determined by wavelength dispersive X-ray fluorescence spectrometry (WD-XRF). Mirror-like polished specimens of $K_{1-x}Pb_{m+\delta}Sb_{1+\gamma}Te_{m+2}$ samples extracted from various locations of the ingot were analyzed using a Bruker AXS, S4 Pioneer X-ray fluorescence spectrometer. High purity ingots of PbTe, Sb_2Te_3, and $KSbTe_2$ were synthesized and used as standards for accurate determination of the chemical composition of $K_{1-x}Pb_{m+\delta}Sb_{1+\gamma}Te_{m+2}$ ingots.

Infrared Spectroscopy. Room temperature optical diffuse reflectance measurements were performed on finely ground powder of $K_{1-x}Pb_{m+\delta}Sb_{1+\gamma}Te_{m+2}$ samples to probe the optical energy band gap of the series. The spectra were monitored in the mid-IR region (6000−400 cm^{-1}) using a Nicolet 6700 FTIR spectrometer. Absorption (α/S) data were calculated from reflectance data using the Kubelka−Munk function as described previously.[27,28] The optical band gaps were derived from α/S versus E (eV) plots.

Thermal Conductivity. The thermal conductivity (κ) was determined as a function of temperature from room temperature to 800 K using the flash diffusivity method on a LFA 457/2/G Microflash, NETZSCH. The front face of a small disk-shaped sample (ϕ = 8 mm; thickness ~1−2 mm) coated with a thin layer of graphite is irradiated by a short laser burst, and the resulting rear face temperature rise is recorded and analyzed. Thermal conductivity (κ) values were calculated using the equation $\kappa = \alpha C_p d$, where α is the thermal diffusivity, C_p is the specific heat (measured using differential scanning calorimetry), and d is the bulk density of the sample (calculated from the sample's geometry and mass). Thermal diffusivity and specific heat data used for the calculation can be found in the Supporting Information. Lattice thermal conductivity was obtained by subtracting the carrier contribution from the total thermal conductivity using the equation $\kappa_{(lattice)} = \kappa_{(total)} - \kappa_{(carrier)}$. Here, $\kappa_{(carrier)}$ is expressed by the Wiedemann−Franz Law $\kappa_{(carrier)} = L\sigma T$, where L is the Lorenz number.

Charge Transport Measurements. Thermopower and electrical conductivity data were obtained from two different sources to ensure reproducibility. Both properties were measured simultaneously using a ZEM-3 Seebeck coefficient/electrical resistivity measurement system (ULVAC-RIKO, Japan) and a homemade four-sample measurement system described elsewhere.[29] The properties were measured for each sample over the selective temperature range of interest. Specimens for thermal conductivity measurements as well as those used for electrical conductivity and thermopower measurements were cut adjacent to one another along the ingot to ensure that the properties are measured along the same direction.

Results and Discussion

Synthesis. Bulk ingots of $K_{1-x}Pb_{m+\delta}Sb_{1+\gamma}Te_{m+2}$ materials are easy to prepare at 100% yield. However, the thermoelectric and mechanical properties of the resulting ingot samples appear to be very sensitive to the cooling profile. This is probably related to a possible composition gradient and internal stresses that may develop across the ingot during cooling and possibly to the variation of the size, shape, and distribution of the nanometer scale inclusions embedded inside the PbTe-rich matrix. The cooling profile reported in this study was found to be the optimum, allowing a high repeatability of mechanically good samples with good thermoelectric properties. It is important to note that a slight change of the surface of the specimen from shiny silver-like appearance to gray occurred during polishing with water. However, after washing and drying with acetone, the surfaces of the specimens regained the original shiny appearance and remained stable for several months under ambient atmosphere.

Several combinations of the compositional parameters x, m, γ, and δ were used to achieve materials with optimum thermoelectric properties. Figure 1 shows the X-ray powder diffraction patterns of samples from the $K_{1-x}Pb_{20+\delta}Sb_{1+\gamma}Te_{22}$ (m = 20) series. Samples with m = 19 and 21 showed similar X-ray diffraction patterns. The cell parameters of $K_{1-x}Pb_{m+\delta}Sb_{1+\gamma}Te_{m+2}$ compounds as a function of the compositional parameters m, x, δ, and γ are given in Table 1. The refined cell parameters (~6.50 Å) are about 0.04 Å larger than that of PbTe (6.459 Å)[30] as would be expected from the difference in the effective ionic radii of Pb (1.19 Å) and K (~1.38 Å).[31] The slight shift of the diffraction peaks toward low 2θ presumably is due to the small additions of excess Sb (or Sb and Pb) into the $K_{1-x}Pb_{20}SbTe_{22}$ matrix. The diffraction patterns indicated that all samples used for this study were single

(27) Chondroudis, K.; McCarthy, T. J.; Kanatzidis, M. G. *Inorg. Chem.* **1996**, *35*, 840–844.
(28) Stephan, H. O.; Kanatzidis, M. G. *Inorg. Chem.* **1997**, *36*, 6050–6057.
(29) Loo, S.; Short, J.; Hsu, K. F.; Kanatzidis, M.; Hogan, T. *Mater. Res. Soc. Symp. Proc.* **2004**, *793*, 375–383.
(30) Bouad, N.; Chapon, L.; Marin-Ayral, R. M.; Bouree-Vigneron, F.; Tedenac, J. C. *J. Solid State Chem.* **2003**, *173*, 189–195.
(31) Shannon, R. D. *Acta Crystallogr., Sect. A* **1976**, *32*, 751–767.

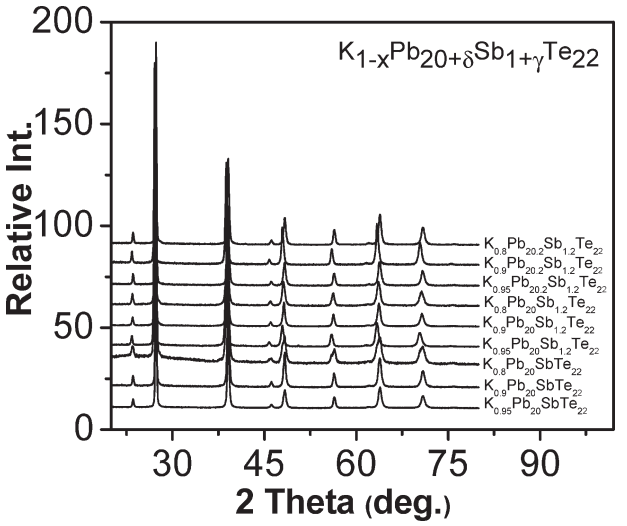

Figure 1. X-ray powder diffraction patterns of $K_{1-x}Pb_{20+\delta}Sb_{1+\gamma}Te_{22}$ ($m = 20$) samples with ($1 - x$, δ, γ): 1 = (0.95, 0, 0); 2 = (0.9, 0, 0), 3 = (0.8, 0, 0); 4 = (0.95, 0, 0.2); 5 = (0.9, 0, 0.2), 6 = (0.8, 0, 0.2); 7 = (0.95, 0.2, 0.2); 8 = (0.9, 0.2, 0.2), 9 = (0.8, 0.2, 0.2). No additional peaks corresponding to elemental Pb or Sb impurities could be observed from the diffraction patterns. All patterns were collected using a Cu Kα (λ = 1.540 56 Å) radiation.

phase with NaCl-type structure. No significant additional peaks from other phases could be detected in the diffraction patterns. Therefore, on the basis of conventional X-ray diffraction these samples appear to be solid solutions. As we will show later this is actually not the case. The average compositions of the $K_{1-x}Pb_{m+\delta}Sb_{1+\gamma}Te_{m+2}$ series obtained from wavelength dispersive X-ray fluorescence analysis were consistent with the nominal compositions.

Thermal Analysis and Optical Band Gap. Figure 2 shows DTA traces of samples with compositions $K_{0.95}Pb_{19}Sb_{1.2}Te_{21}$ (1), $K_{0.95}Pb_{20}Sb_{1.2}Te_{22}$ (2), and $K_{0.95}Pb_{21}Sb_{1.2}Te_{23}$ (3). All DTA curves show only one endothermic peak of the melting during the heating cycle and one exothermic peak of crystallization on the cooling cycle, indicating again congruent melting materials. The melting temperature (peak temperature) is ~1200 K for all samples and the crystallization temperature is ~1130 K for samples with $m = 20$ and 21 while the composition with $m = 19$ crystallized at much lower temperature (1090 K).

Infrared spectroscopy of $K_{1-x}Pb_{m+\delta}Sb_{1+\gamma}Te_{m+2}$ series of compounds showed that all members of the series are narrow gap semiconductors. Typical absorption spectra for the $K_{1-x}Pb_{20+\delta}Sb_{1+\gamma}Te_{22}$ ($m = 20$) series are shown in Figure 3. Similar spectra were observed for samples with $m = 19$ and 21. All spectra show sharp well-defined change in the absorption coefficient. The band gaps derived from these plots are $E_g \sim 0.32$ eV for all compositions. This value is about 0.03 eV larger than that of pure PbTe ($E_g = 0.29$ eV).[32] This increase in the band gap of $K_{1-x}Pb_{m+\delta}Sb_{1+\gamma}Te_{m+2}$ is consistent with the possible formation of isostructural compounds between the narrow gap semiconductor PbTe and a wider gap $KSbTe_2$ material ($E_g \sim 0.55$ eV). The larger band gap of $K_{1-x}Pb_{m+\delta}Sb_{1+\gamma}Te_{m+2}$ is particularly attractive because the gap crossover by thermally excited carriers that ultimately leads to a maximum in ZT will be pushed to higher temperatures. This result, combined with the high melting temperature of $K_{1-x}Pb_{m+\delta}Sb_{1+\gamma}Te_{m+2}$, significantly enhances the potential of these materials for high temperature energy conversion application.

Transmission Electron Microscopy. The $K_{1-x}Pb_{m+\delta}Sb_{1+\gamma}Te_{m+2}$ series of compounds as highlighted above is susceptible to develop nanoscale features embedded inside the bulk matrix. Because of the K^+/Sb^{3+} replacement of Pb^{2+} atoms in the rock salt structure, there is a tendency (being mainly of electrostatic origin) to form alkali metal/antimony clusters as proposed previously.[4,5] In addition, the presence of a slight excess of Sb predisposes this series of materials to various kinds of nano/micro features that can be better assessed by transmission electron microscopy. The microstructures of several specimens from numerous ingots of the $K_{1-x}Pb_{m+\delta}Sb_{1+\gamma}Te_{m+2}$ series were examined under high resolution transmission electron microscopy (HRTEM). Figure 4 shows typical low magnification and high magnification HRTEM images of specimens from samples with composition $K_{0.95}Pb_{20}SbTe_{22}$ and $K_{0.95}Pb_{20}Sb_{1.2}Te_{22}$, respectively. Similar images were observed in specimens from various other compositions of $K_{1-x}Pb_{m+\delta}Sb_{1+\gamma}Te_{m+2}$. Low magnification images (Figure 4a,c) clearly revealed the presence of nanometer size particles coherently (endotaxy) embedded inside the matrix. The nanocrystals are of various shape and size and are randomly oriented. The typical particle size is between 3 and 10 nm.

Although we did not perform elemental analysis on the nanoinclusions, we anticipate based on the chemistry of the system that they should be K and Sb-rich. High magnification images (Figure 4b,d) also suggested that the particles form a coherent interface with the matrix. This is a very desirable feature as it allows transparent flow of electrons through the nanocrystals which preserves the electrical conductivity of the materials. Simultaneously, the nanocrystals, because of high mass contrast with the matrix, can act as barriers to thermal phonons. The phonon blocking power of $K_{1-x}Pb_{m+\delta}Sb_{1+\gamma}Te_{m+2}$ materials is expected to be enhanced by the apparent high density of the nanoinclusions (Figure 4) as well as by their wide size distribution (from ~2 to ~20 nm), which allow for the scattering of a broad range of the phonon spectrum (mid- to long wavelength). As we will see below, this indeed leads to significantly reduced lattice thermal conductivity for the PLAT-m materials.

Lattice Thermal Conductivity. Figure 5 shows the temperature dependence of the total thermal conductivity (κ) and the lattice thermal conductivity (κ_L) of the $K_{1-x}Pb_{m+\delta}Sb_{1+\gamma}Te_{m+2}$ series of samples. Regardless of the m value, the total thermal conductivity of $K_{1-x}Pb_{m+\delta}Sb_{1+\gamma}Te_{m+2}$ samples varies from 2.4 to 1.4 W/(m·K) at 300 K (Figure 5a−c). The room temperature values of the lattice thermal conductivity for samples with $m = 19$ range from 1 W/(m·K) for the

(32) Koppensteiner, E.; Springholz, G.; Hamberger, P.; Bauer, G. *J. Appl. Phys.* **1993**, *74*, 6062–6071.

Table 1. Lattice Parameters of $K_{1-x}Pb_{m+\delta}Sb_{1+\gamma}Te_{m+2}$ (m = 19, 20, 21) Samples Refined from X-ray Powder Diffraction Data

m = 19		m = 20		m = 21	
$(1-x, \delta, \gamma)$	a (Å)	$(1-x, \delta, \gamma)$	a (Å)	$(1-x, \delta, \gamma)$	a (Å)
		(0.95, 0, 0)	6.508(3)	(0.95, 0, 0)	6.505(3)
(0.9, 0, 0)	6.463(3)	(0.9, 0, 0)	6.507(3)	(0.9, 0, 0)	6.506(3)
(0.8, 0, 0)	6.464(4)	(0.8, 0, 0)	6.500(3)	(0.8, 0, 0)	6.504(4)
(0.95, 0, 0.2)	6.507(3)	(0.95, 0, 0.2)	6.501(1)	(0.95, 0, 0.2)	6.485(4)
(0.9, 0, 0.2)	6.501(2)	(0.9, 0, 0.2)	6.506(2)	(0.9, 0, 0.2)	6.486(3)
(0.8, 0, 0.2)	6.508(2)	(0.8, 0, 0.2)	6.500(3)	(0.8, 0, 0.2)	6.484(3)
(0.95, 0.2, 0.2)	6.508(1)	(0.95, 0.2, 0.2)	6.508(2)	(0.95, 0.2, 0.2)	6.507(2)
(0.9, 0.2, 0.2)	6.501(3)	(0.9, 0.2, 0.2)	6.502(5)	(0.9, 0.2, 0.2)	6.500(3)
(0.8, 0.2, 0.2)	6.507(3)	(0.8, 0.2, 0.2)	6.507(2)	(0.8, 0.2, 0.2)	6.505(3)

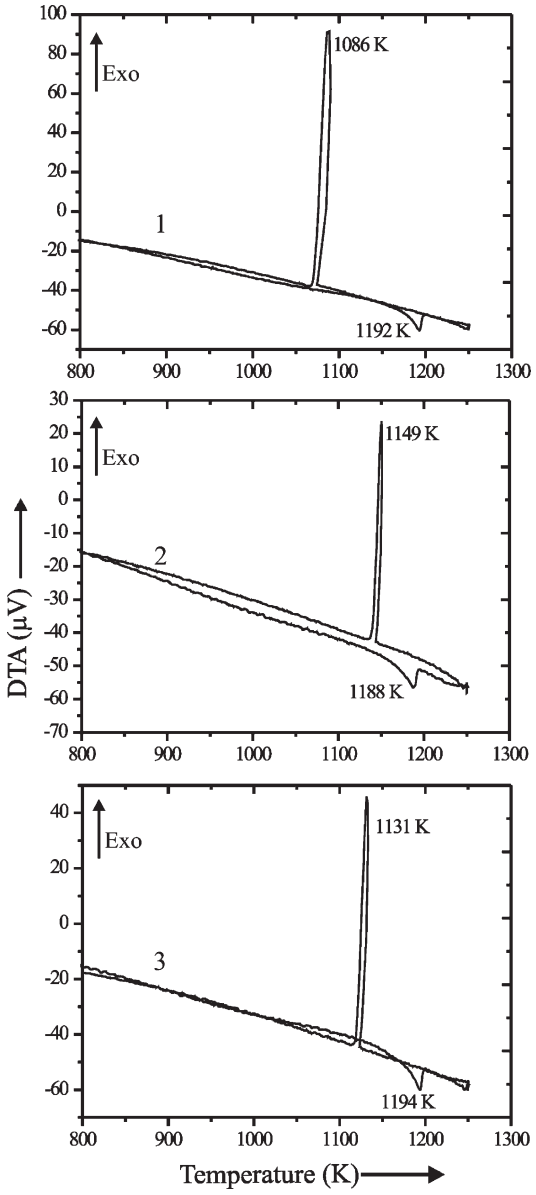

Figure 2. DTA traces of $K_{0.95}Pb_mSb_{1.2}Te_{m+2}$ samples showing peaks of melting and recrystallization. 1: m = 19; 2: m = 20; 3: m = 21. No additional peaks of excess elemental Sb could be detected. Heating rate 10 K/min.

composition $K_{0.8}Pb_{19}Sb_{1.2}Te_{21}$ to 0.6 W/(m·K) for sample $K_{0.8}Pb_{19.2}Sb_{1.2}Te_{21}$ (Figure 5d). These values are

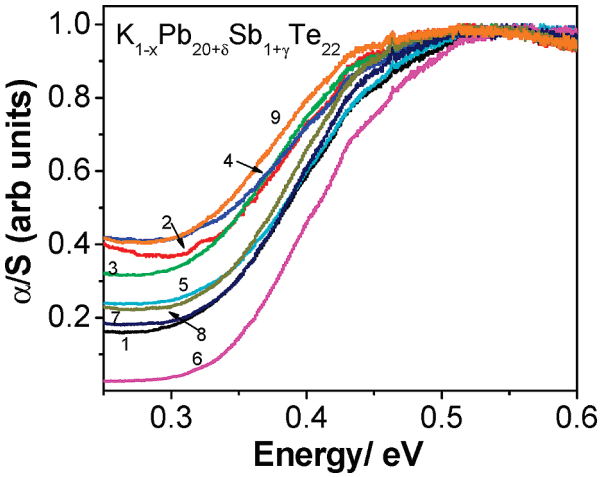

Figure 3. Infrared absorption spectra of $K_{1-x}Pb_{20+\delta}Sb_{1+\gamma}Te_{22}$ (m = 20) samples with $(1-x, \delta, \gamma)$: 1 = (0.95, 0, 0); 2 = (0.9, 0, 0), 3 = (0.8, 0, 0); 4 = (0.95, 0, 0.2); 5 = (0.9, 0, 0.2), 6 = (0.8, 0, 0.2); 7 = (0.95, 0.2, 0.2); 8 = (0.9, 0.2, 0.2), 9 = (0.8, 0.2, 0.2). The band gaps are similar and range from 0.32 eV (1) to 0.34 eV (6).

two to four times lower than the typical lattice thermal conductivity of undoped PbTe (2.3 W/(m·K)).[33−37] The lattice thermal conductivity decreases with increasing temperature. At 550 K the values are between 0.4 and 0.7 W/(m·K). Similar values of the lattice thermal conductivity were obtained for samples with m = 20 and 21 (Figures 5e,f). For samples with compositions $K_{1-x}Pb_{20}Sb_{1.2}Te_{22}$, the lattice thermal conductivity clearly decreases with increasing K content $(1-x)$ (Figure 5e), suggesting a varying concentration of $KSbTe_2$-rich nanocrystals within the PbTe-rich matrix. The room temperature values of the lattice thermal conductivity decrease from 1.2 W/(m·K) for $K_{0.8}Pb_{20}Sb_{1.2}Te_{22}$ to 0.7 W/(m·K) for $K_{0.95}Pb_{20}Sb_{1.2}Te_{22}$. For the samples with compositions $K_{0.95}Pb_{20}Sb_{1.2}Te_{22}$ and $K_{0.95}Pb_{21.2}Sb_{1.2}Te_{23}$, a record low value of 0.2 W/(m·K) was achieved at 600 K (caution: this value derives from a Lorenz number of 2.45×10^{-8} W·Ω/K^2 and could be underestimated given the known tendency of this number to decrease with rising temperature).

(33) Martin, J.; Nolas, G. S.; Zhang, W.; Chen, L. *Appl. Phys. Lett.* **2007**, *90*, 222112.
(34) Orihashi, M.; Noda, Y.; Kaibe, H. T.; Nishida, I. A. *Mater. Trans.* **1998**, *39*, 672–678.
(35) Orihashi, M.; Noda, Y.; Chen, L.; Hirai, T. *J. Jpn. Inst. Met.* **1999**, *63*, 1423–1428.
(36) Orihashi, M.; Noda, Y.; Chen, L. D.; Hirai, T. *Mater. Trans.* **2000**, *41*, 1282–1286.
(37) Orihashi, M.; Noda, Y.; Chen, L. D.; Hirai, T. *Mater. Trans.* **2000**, *41*, 1196–1201.

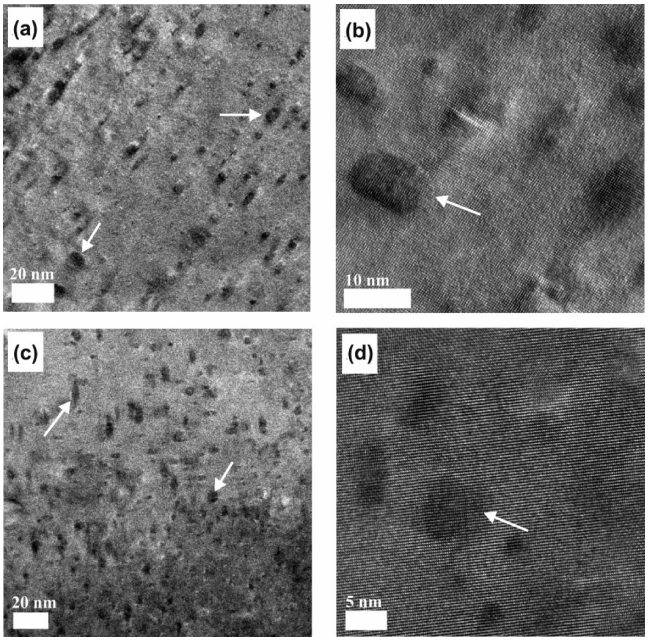

Figure 4. Selected HRTEM images of $K_{1-x}Pb_{20+\delta}Sb_{1+\gamma}Te_{22}$ (m = 20) samples. (a) Low magnification TEM image of $K_{0.95}Pb_{20}SbTe_{22}$ showing nanometer size crystalline K/Sb-rich particles coherently embedded in a PbTe-rich matrix. (b) The corresponding high magnification image showed coherently particles/matrix boundaries. (c) Low magnification TEM image of $K_{0.95}Pb_{20}Sb_{1.2}Te_{22}$ indicating the degree of dispersion of nanometer size particles in PbTe-rich matrix. (d) The corresponding high resolution version showing well crystallized particles coherent to the matrix.

We note that these numbers are based on a Lorenz number of 2.45×10^{-8} W·Ω/K^2 assumed to be constant with temperature. The Lorenz number may be lower than that and probably also varies with temperature, but we have no experimental estimate of it. Therefore, if the experimental Lorenz numbers for these materials are determined in future studies, these values of the lattice thermal conductivity should be re-evaluated on the basis of the electrical conductivities of the corresponding samples reported here. For example, assuming a Lorenz number of 1.2×10^{-8} W·Ω/K^2 at 600 K the lattice thermal conductivity of the compositions $K_{0.95}Pb_{20}Sb_{1.2}Te_{22}$ and $K_{0.95}Pb_{21.2}Sb_{1.2}Te_{23}$ is still a record low value (for semiconductors) of 0.4 W/(m·K).

Despite the uncertainty in the Lorenz number, a strong reduction of the lattice thermal conductivity of the $K_{1-x}Pb_{m+\delta}Sb_{1+\gamma}Te_{m+2}$ series of samples below the PbTe "alloys limits" is evident from our data and is a strong indication of the significant contribution of embedded nanostructures (observed from HRTEM) to the scattering of thermal phonons. The typical room temperature value of the lattice thermal conductivity of solid solutions materials based on PbTe is around 1.5 W/(m·K).[35,36,38] This result is in line with the low lattice thermal conductivity values reported recently for the $Na_{1-x}Pb_mSbTe_{m+2}$ and suggests that alkali metals dopands provide additional scattering power to the PbTe-based materials over the coinage metals dopands.

(38) Devyatko, E.; Tikhonov, V. V. *Soviet Physics Solid State, USSR* **1965**, *7*, 1427–+.

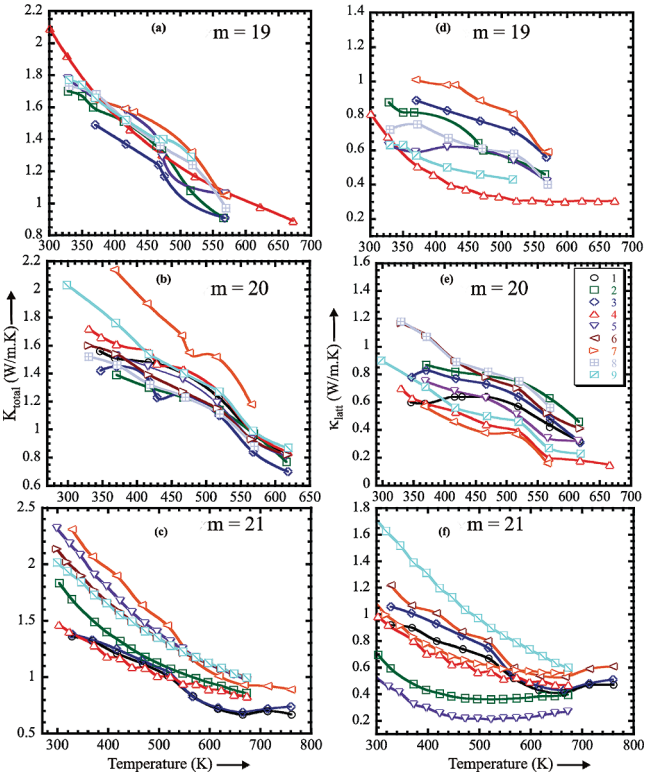

Figure 5. Temperature dependence of the total thermal conductivity (a, b, and c) and the lattice thermal conductivity (d, e, and f) of $K_{1-x}Pb_{m+\delta}Sb_{1+\gamma}Te_{m+2}$ (m = 19, 20, and 21) samples. ($1-x$, δ, γ): 1 = (0.95, 0, 0); 2 = (0.9, 0, 0), 3 = (0.8, 0, 0); 4 = (0.95, 0, 0.2); 5 = (0.9, 0, 0.2), 6 = (0.8, 0, 0.2); 7 = (0.95, 0.2, 0.2); 8 =(0.9, 0.2, 0.2), 9 = (0.8, 0.2, 0.2).

Electrical Properties. The $K_{1-x}Pb_{m+\delta}Sb_{1+\gamma}Te_{m+2}$ series of compounds in addition to the very low lattice thermal conductivity shows promising electrical properties. Figures 6, 7, and 8 show the temperature dependence of the electrical conductivity, thermopower, power factor, and figure of merit of $K_{1-x}Pb_{19+\delta}Sb_{1+\gamma}Te_{21}$ (m = 19), $K_{1-x}Pb_{20+\delta}Sb_{1+\gamma}Te_{22}$ (m = 20), and $K_{1-x}Pb_{21+\delta}Sb_{1+\gamma}Te_{23}$ (m = 21), respectively. The room temperature values of the electrical conductivity of samples with m = 19 (Figure 6a) range from 1000 S/cm for the composition $K_{0.8}Pb_{19}Sb_{1.2}Te_{21}$ to 1800 S/cm for $K_{0.95}Pb_{19.2}Sb_{1.2}Te_{21}$. Similar values were measured for samples with m = 20 and 21 (Figures 7a and 8a). Depending on the values of the composition parameters (δ and γ), various dependences of the electrical conductivity on the K concentrations were observed. For the sample with composition $K_{1-x}Pb_{19}Sb_{1.2}Te_{21}$, for example, the electrical conductivity decreased with decreasing K concentration while samples in which excess of both Sb and Pb were present such as $K_{1-x}Pb_{19.2}Sb_{1.2}Te_{21}$ showed increase in the electrical conductivity with decreasing K concentration. Similar trends were observed for samples with m = 20 and 21 (Figures 7a and 8a). Within a given m, the electrical conductivity at temperatures below 500 K is very sensitive to the change in composition parameters ($1-x$, δ, γ). The conductivity curves, however, converge at temperatures above 500 K. For all samples, the electrical conductivity decreases monotonically as the temperature rises indicating degenerate conduction for the whole measuring temperature range.

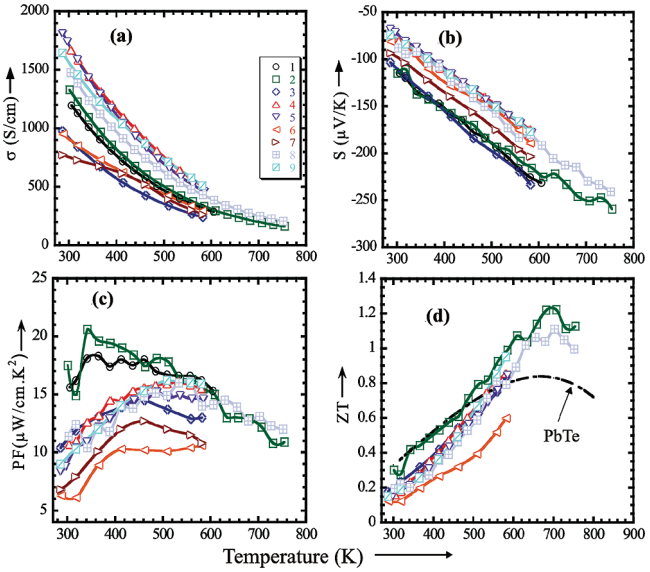

Figure 6. Temperature dependence of the thermoelectric properties of $K_{1-x}Pb_{19+\delta}Sb_{1+\gamma}Te_{21}$ (m = 19) samples. Electrical conductivity (a), thermopower (b), power factor (c), and figure of merit (d); ($1-x$, δ, γ): 1 = (0.95, 0, 0); 2 = (0.9, 0, 0), 3 = (0.8, 0, 0); 4 = (0.95, 0, 0.2); 5 = (0.9, 0, 0.2), 6 = (0.8, 0, 0.2); 7 = (0.95, 0.2, 0.2); 8 = (0.9, 0.2, 0.2), 9 = (0.8, 0.2, 0.2).

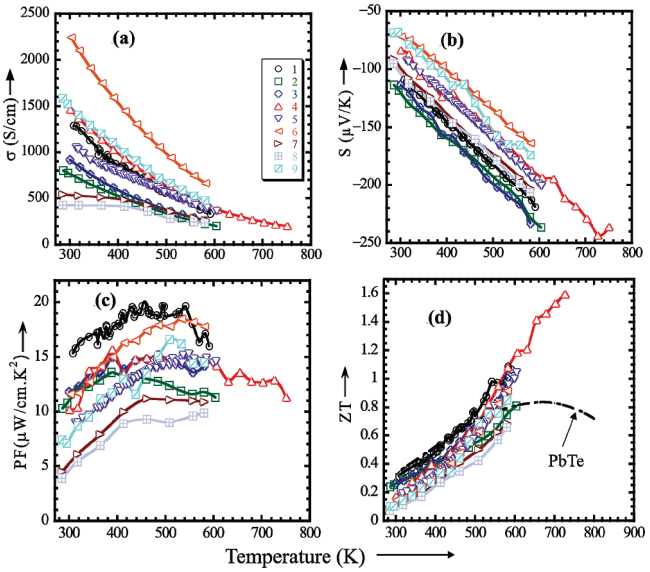

Figure 7. Temperature dependence of the thermoelectric properties of $K_{1-x}Pb_{20+\delta}Sb_{1+\gamma}Te_{22}$ (m = 20) samples. Electrical conductivity (a), thermopower (b), power factor (c), and figure of merit (d); ($1-x$, δ, γ): 1 = (0.95, 0, 0); 2 = (0.9, 0, 0), 3 = (0.8, 0, 0); 4 = (0.95, 0, 0.2); 5 = (0.9, 0, 0.2), 6 = (0.8, 0, 0.2); 7 = (0.95, 0.2, 0.2); 8 = (0.9, 0.2, 0.2), 9 = (0.8, 0.2, 0.2).

Most PbTe-based materials show electrical conductivity that follows the power law $T^{-\lambda}$ (λ = 2.3−2.5).[39] The temperature dependence of the electrical conductivity of the $K_{1-x}Pb_{m+\delta}Sb_{1+\gamma}Te_{m+2}$ materials seems to follow the same dependence, although the fits to a power law were not perfect (Table 2). The importance of the power exponent and its influence on the power factor were

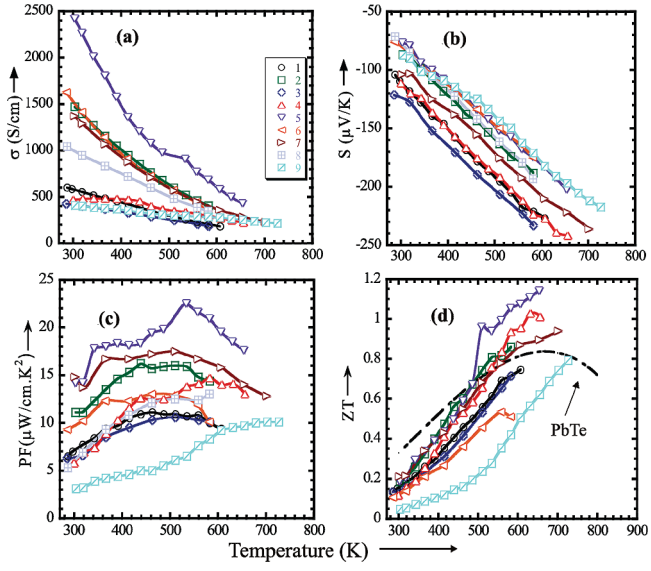

Figure 8. Temperature dependence of the thermoelectric properties of $K_{1-x}Pb_{21+\delta}Sb_{1+\gamma}Te_{23}$ (m = 21) samples. Electrical conductivity (a), thermopower (b), power factor (c), and figure of merit (d); ($1-x$, δ, γ): 1 = (0.95, 0, 0); 2 = (0.9, 0, 0), 3 = (0.8, 0, 0); 4 = (0.95, 0, 0.2); 5 = (0.9, 0, 0.2), 6 = (0.8, 0, 0.2); 7 = (0.95, 0.2, 0.2); 8 = (0.9, 0.2, 0.2), 9 = (0.8, 0.2, 0.2).

recently discussed previously in another nanostructured thermoelectric material system.[40]

The surprising finding in this material system came from the thermopower measurements. Contrary to the sodium containing materials which show positive thermopower indicating p-type behavior, all $K_{1-x}Pb_{m+\delta}Sb_{1+\gamma}Te_{m+2}$ materials exhibit n-type conduction as indicated by the negative values of the thermopower. Although it is difficult to explain the switch in conduction type from p- to n-type in moving from Na to K, we can glean some insight from the recently reported discrepancy in the electronic structure of PbTe around the Fermi level when doped with a single impurity of Na or K. The theoretical study suggested that an addition of a single K impurity in PbTe increases the density of state (DOS) at the top of the valence band while Na impurities show no perturbation of the electronic structure around the Fermi level.[24] This result can be regarded as a calibration scale to understand how Na and K dope PbTe p-type. Apparently, the addition of Sb which is an n-type dopand for PbTe drives more easily a K containing PbTe system to n-type behavior. A test experiment aimed at converting the p-type system $Na_{1-x}Pb_mSb_yTe_{m+2}$ into n-type showed that a high Sb/Na ratio is required. For example, the composition $Na_{0.95}Pb_{20}Sb_{1.5}Te_{22}$ showed n-type behavior with a room temperature thermopower of −125 μV/K and an electrical conductivity of 700 S/cm.

The room temperature thermopower values for $K_{1-x}Pb_{19+\delta}Sb_{1+\gamma}Te_{21}$ (m = 19) range from −70 μV/K to −100 μV/K (Figure 6b). The thermopower of all samples increases almost linearly with rising temperature. For the $K_{1-x}Pb_{19+\delta}Sb_{1+\gamma}Te_{21}$ series of samples, the thermopower increases with increasing K concentration for constant values of δ and γ (Figure 6b). For a given K concentration, the thermopower decreases when excesses

(39) Ravich, Y. I.; Efimova, B. A.; Smirov, I. A. *Semiconducting Lead Chalcogenides*; Plenum Press: New York, 1970; p 155.
(40) Sootsman, J. R.; Kong, H. J.; Uher, C.; D'Angelo, J. J.; Wu, C. I.; Hogan, T. P.; Caillat, T.; Kanatzidis, M. G. *Angew. Chem., Int. Ed.* **2008**, *47*, 8618−8622.

Table 2. Temperature Dependence of the Electrical Conductivity of $K_{1-x}Pb_{m+\delta}Sb_{1+\gamma}Te_{m+2}$ (m = 19, 20, 21) Samples on Temperature[a]

m = 19		m = 20		m = 21	
$(1-x, \delta, \gamma)$	λ	$(1-x, \delta, \gamma)$	λ	$(1-x, \delta, \gamma)$	λ
(0.95, 0, 0)	2.10	(0.95, 0, 0)	1.91	(0.95, 0, 0)	1.55
(0.9, 0, 0)	2.35	(0.9, 0, 0)	1.81	(0.9, 0, 0)	1.95
(0.8, 0, 0)	2.00	(0.8, 0, 0)	1.90	(0.8, 0, 0)	1.14
(0.95, 0, 0.2)	1.81	(0.95, 0, 0.2)	2.23	(0.95, 0, 0.2)	0.98
(0.9, 0, 0.2)	1.89	(0.9, 0, 0.2)	1.59	(0.9, 0, 0.2)	2.14
(0.8, 0, 0.2)	1.62	(0.8, 0, 0.2)	1.85	(0.8, 0, 0.2)	2.11
(0.95, 0.2,0.2)	1.50	(0.95, 0.2,0.2)	0.99	(0.95, 0.2, 0.2)	2.10
(0.9, 0.2, 0.2)	2.19	(0.9, 0.2, 0.2)	0.91	(0.9, 0.2, 0.2)	1.55
(0.8, 0.2, 0.2)	1.62	(0.8, 0.2, 0.2)	1.66	(0.8, 0.2, 0.2)	0.70

[a] $\sigma \sim T^{-\lambda}$.

Sb or Sb and Pb are added to the $K_{1-x}Pb_{19}SbTe_{21}$ matrix. At 700 K, a thermopower value of -260 μV/K was measured for the sample with composition $K_{0.9}Pb_{19}SbTe_{21}$ resulting in a power factor of 13 $\mu W/(cm \cdot K^2)$ at 700 K. (Figure 6c).

For the series of samples with m = 20, stronger dependence of the thermopower on the composition parameters $1-x$, δ, and γ was observed (Figure 7b). The thermopower increases with increasing K concentration for constant values of δ and γ. For m = 20, the room temperature values of the thermopower range from -70 μV/K to -110 μV/K and increase linearly with temperature. The composition $K_{0.9}Pb_{20}SbTe_{22}$ exhibited the largest thermopower (-240 μV/K at 650 K) for this series of samples (Figure 7b); however, the highest power factor at 650 K ($\sim$17 $\mu W/cm \cdot K^2$) was obtained for $K_{0.9}Pb_{20}Sb_{1.2}Te_{22}$ (Figure 7c) because of the considerably higher electrical conductivity ($\sim$500 S/cm) at 650 K. Samples from the m = 21 series (Figure 8b,c) show similar behavior to those of the m = 20 series. For a given value of m, the thermopower of the $K_{1-x}Pb_{m+\delta}Sb_{1+\gamma}Te_{m+2}$ materials generally increased with the K/Sb ratio. For samples with fixed K/Sb ratio, there was only a marginal fluctuation on the thermopower when changing the value of m.

The temperature dependences of ZT for samples of the series $K_{1-x}Pb_{m+\delta}Sb_{1+\gamma}Te_{m+2}$ are compared in Figures 6d, 7d, and 8d with that of the n-type PbTe reference material. The room temperature ZT values for samples with m = 19 and m = 21 range from 0.1 to 0.2 (Figures 6d and 8d). This is about 1/3 to 2/3 of the value reported for the best doped PbTe and is about two times lower than that of the LAST-18 composition.[4,19] However, ZT plots of PLAT-m materials show very strong temperature dependence compared to doped PbTe and LAST-18. As the temperature rises, the ZT increases rapidly reaching $\sim$1 around 600 K. Most compositions with m = 19 and m = 21 follow this trend (Figures 6d and 8d). The highest ZT of 1.2 was obtained at 700 K for the compositions $K_{0.9}Pb_{19}SbTe_{21}$ and $K_{0.9}Pb_{21}Sb_{1.2}Te_{23}$. The ZT plots of samples from the $K_{1-x}Pb_{20+\delta}Sb_{1+\gamma}Te_{22}$ (m = 20) series also follow the trend described above for samples of the $K_{1-x}Pb_{19+\delta}Sb_{1+\gamma}Te_{21}$ (m = 19) and $K_{1-x}Pb_{19+\delta}Sb_{1+\gamma}Te_{21}$ (m = 21) series.

The most significant enhancement of ZT was observed for the composition $K_{0.95}Pb_{20}Sb_{1.2}Te_{22}$ (Figure 7d). The ZT was 0.2 at 300 K and increased quickly with temperature exceeding PbTe (ZT $\sim$ 0.8) around 500 K and reached the highest value $\sim$1.6 at 750 K. This value is two times larger than the value reported for n-type PbTe and equals the performance of LAST-18. The enhanced figure of merit of $K_{1-x}Pb_{m+\delta}Sb_{1+\gamma}Te_{m+2}$ materials derives from an unusual combination of the moderately high power factor with an impressively low lattice thermal conductivity. The $K_{1-x}Pb_{m+\delta}Sb_{1+\gamma}Te_{m+2}$ materials system holds great promise for successful scale up as only marginal change of the properties is observed upon small variation of the composition.

Concluding Remarks

The $K_{1-x}Pb_{m+\delta}Sb_{1+\gamma}Te_{m+2}$ materials system (PLAT-m) offers additional proof of the strong influence of the alkali-metal on the reduction of the lattice thermal conductivity of PbTe-based materials. To date two modalities of nanostructuring have emerged, "nanodot in a matrix"[5] and pressed nanocrystalline ensembles.[11,33] The first kind involves nanodots which may be coherent with the matrix (endotaxy) or incoherent. The PLAT system we describe here is an endotaxially nanostructured material with well-defined "nanodot in a matrix" character. All compositions show significantly reduced lattice thermal conductivity with moderate electrical conductivity and thermopower. As a result, a maximum ZT of $\sim$1.60 at 750 K was achieved for the composition $K_{0.95}Pb_{20}Sb_{1.2}Te_{22}$. This value is twice that of the state-of- the-art n-type PbTe and equals that of the n-type LAST-18 materials. Combined HRTEM and thermal conductivity data on $K_{1-x}Pb_{m+\delta}Sb_{1+\gamma}Te_{m+2}$ and $Na_{1-x}Pb_mSbTe_{m+2}$, LAST-m and LASTT-m systems (m = 18$-$21), suggest that alkali-metal based PbTe materials exhibit significantly reduced thermal conductivity compared to the LAST-m analogue system. The primary reason for this is the strong tendency of alkali-metal and Sb to promote the formation of stable nanocrystals that are coherently embedded in the PbTe-rich matrix and serve as additional phonon scattering centers with less impact on the electron flow.[26] In addition, the stability of the thermoelectric properties of $K_{1-x}Pb_{m+\delta}Sb_{1+\gamma}Te_{m+2}$ and $Na_{1-x}Pb_mSbTe_{m+2}$ materials upon small variation of the composition is a strong indication of successful scale-up synthesis. The low cost of alkali-metal compared to the cost of silver is another strong advantage of the $K_{1-x}Pb_{m+\delta}Sb_{1+\gamma}Te_{m+2}$ (n-type) and $Na_{1-x}Pb_mSbTe_{m+2}$ (p-type) over the silver-based materials LAST-m (n-type) and LASTT-m (p-type).

Acknowledgment. Financial support from the Office of Naval Research (NO0014-08-0613) is greatly acknowledged. We thank Robert Pcionek for his assistance with TEM.

Supporting Information Available: Figures and tables of diffusivity and specific heat data (PDF). This material is available free of charge via the Internet at http://pubs.acs.org.